TOWARDS UNDERWATER IMAGE RESTORATION: A PHYSICAL-ACCURATE PIPELINE AND A LARGE SCALE FULL-REFERENCE BENCHMARK

Jiayan Tong[1], Lin Zhang[2,], Tianjun Zhang[2]*

[1]School of Electronic and Information Engineering, Tongji University, Shanghai, China
[2]School of Software Engineering, Tongji University, Shanghai, China

ABSTRACT

Underwater images always present low-quality features such as low contrast, blurred edges and color distortion, which brings great challenges to high-level underwater vision tasks. In this paper, a novel underwater image restoration method, namely MonoUIR (Monocular Underwater Image Restoration), is proposed, which is based on a more physical-accurate imaging model compared to existing schemes. And with the monocular depth estimation, MonoUIR has no dependence on extra ranging equipment or specific shooting operations. Experimental results demonstrate that MonoUIR overwhelmingly outperforms other physical model-based competitors. In addition, the Real-world Undersea Color Board (RUCB) dataset is established, providing the ill-conditioned underwater images collected in the East China Sea and the corresponding high-quality references. To our knowledge, this is the first full-reference underwater benchmark dataset collected entirely in a real-world marine environment, which will further support the full-reference evaluation of underwater image restoration approaches. The source code and the dataset are available at https://TongJiayan.github.io/MonoUIR-Homepage.

Index Terms— Underwater image restoration, monocular depth estimation, full-reference, benchmark

1. INTRODUCTION

Due to the wavelength-dependent absorption and scattering of light when propagating in seawater, underwater images generally present low-quality features, including low contrast, blurred edges and color distortion, which significantly increases the difficulty of high-level underwater computer vision tasks. To improve the usability of underwater visual data, many restoration methods have already been proposed, aiming to eliminate or partially eliminate the degradation of underwater images, and obtain restored images that are close to those captured in the air.

The existing model-based restoration methods generally can not achieve satisfactory performance, which is manifested as inaccurate color restoration, incomplete deblurring and poor generalization. One of the causes is that the underwater imaging model these methods depend on follows an ideal assumption, in which the direct signal and the backscattering signal are governed by the same uniform attenuation coefficient. Moreover, some existing restoration methods rely on extra ranging equipment or multiple images captured from different perspectives to obtain depth information. Consequently, these methods can not work as expected for most existing underwater images due to the lack of depth maps.

Another research gap is that the existing restoration methods generally can only be evaluated by non-reference assessments [1, 2], which just take the inherent quality of the restored image into accounts, such as contrast and color density, while hardly considering how close the restored image is to the real-world scene. The leading cause is the lack of underwater image datasets that can provide corresponding references simultaneously.

As an attempt to fill in the aforementioned research gaps to some extent, we propose a novel underwater image restoration approach, namely MonoUIR (Monocular Underwater Image Restoration). Compared with existing schemes, it's more physically accurate and doesn't rely on any ranging equipment. Besides, the first full-reference underwater dataset, RUCB (Real-world Undersea Color Board), is established, which can provide solid support to the evaluation of underwater image restoration approaches. In summary, the main contributions of this paper are summarized as follows,

- A novel underwater single image restoration method MonoUIR is proposed. It utilizes a physical-accurate and robust imaging model, in which the attenuation coefficients are signal-distinguished and adaptive to the depth. Besides, by integrating the monocular depth estimation, MonoUIR has no dependence on extra ranging equipment or specific shooting operations.

- The Real-world Undersea Color Board (RUCB) dataset is established, consisting of ill-conditioned underwater images collected in the East China Sea and the non-degraded references. To our knowledge, this is the first full-reference underwater dataset completely collected in the real world.

---

*Corresponding author. Email: cslinzhang@tongji.edu.cn

- Both existing underwater image restoration methods and our proposed MonoUIR are evaluated in a full-reference manner, which is rare in previous work due to the lack of data support. Actually, this is a more reliable solution to evaluate the performance of underwater image restoration schemes.

2. RELATED WORK

Underwater image restoration has been a long-standing problem, with great progress made over the past decade. Here we make a review on existing underwater image restoration schemes and relevant public datasets.

Underwater image restoration. Existing underwater image restoration methods mainly fall into two categories: physical model-based ones and data-driven ones. The physical model-based methods [3–5] usually estimate the parameters of the degradation model with observation data or various priors, aiming to reverse the degradation of underwater imaging. These methods generally adopt the imaging model which assumes the direct and the backscattering signals are governed by the same uniform attenuation coefficient. This ideal assumption will have a negative impact on the accuracy and robustness of restoration.

As another attempt on underwater image restoration, the data-driven schemes [6–8] are inspired by deep learning techniques and highly dependent on large-scale training datasets. It's worth mentioning that, to address the lack of paired training data, these schemes usually introduce GAN (Generative Adversarial Network) to generate underwater images from in-air images and depth pairings. Nevertheless, due to the limitations of multiple possible outputs from GANs and the gap between synthesized underwater images and real-world ones, the robustness and the generalization capability of existing data-driven methods still fall behind model-based state-of-the-art methods.

Underwater image datasets. Underwater image datasets are significant for designing and evaluating underwater image restoration methods. Several real-world underwater image datasets [9–11] have been released, which were collected in the real-world marine environment. However, the content of these datasets is relatively monotonous. For example, the seathru dataset [11] contains thousands of underwater images, but only covers five different scenes. Moreover, since it is quite challenging to obtain the non-degraded ground truth of real-world underwater images,these datasets have no reference images provided. To sidestep this problem, Duarte *et al.* [12] simulated the marine environment using milk in a tank. Although in Duarte *et al.*'s dataset, paired underwater images and references are provided, there is still a non-negligible gap between the real-world environment and the simulated one. Overall, there is no full-reference underwater dataset entirely collected from the real world yet.

3. PROPOSED METHOD

In this section, the workflow of MonoUIR will be presented in detail. Firstly, the underwater imaging model will be introduced in Sect. 3.1. Then, how to estimate the parameters of the model will be described in the following three subsections. The pipeline of MonoUIR is illustrated in Fig. 1.
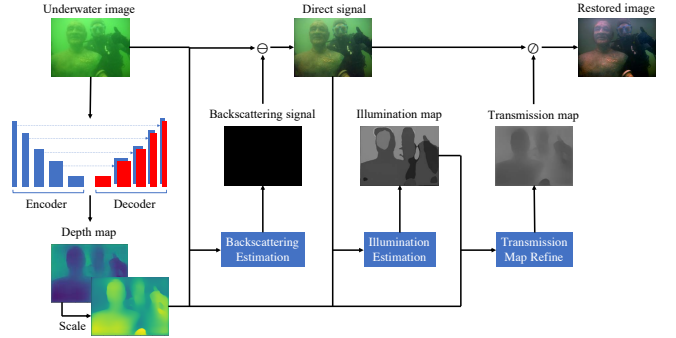
Fig. 1. The pipeline of our MonoUIR. "⊖" and "⊘" indicate the subtraction and division operation, respectively.

3.1. Underwater Imaging Model

Underwater imaging models usually regard the image signal I_c as the combination of the direct signal D_c reflected from objects and the backscattering signal B_c, which is the signal of ambient light scattered by marine particles. Different from the underwater imaging model widely used by existing model-based methods, which assumes the direct signal and the backscattering signal are governed by the same uniform attenuation coefficient, the model proposed in [13] claims that the attenuation coefficient of the backscatter is different from that of the direct transmission, and builds the physically valid space of the attenuation coefficients with oceanographic techniques. This model can be formulated as,

$$
\begin{aligned}
I_c &= D_c + B_c \\
&= J_c * e^{-\beta_c^D(v_D)*z} + A_c * \left(1 - e^{-\beta_c^B(v_B)*z}\right)
\end{aligned}
\tag{1}
$$

where J_c represents the restored image without degradation, β_c^D and β_c^B represent the attenuation coefficients governing the direct signal and the backscattering signal, respectively, z represents the depth map, A_c denotes ambient light, and vector v_D and v_B represent the parameters on which β_c^D and β_c^B depend, respectively, including equipment parameters and environmental ones that are usually difficult to obtain.

According to Eq. (1), we have to know all environmental parameters as well as equipment ones so as to obtain the restored image J_c, which is impractical for most cases. From this point, in order to reduce the complexity of parameter estimation, we simplify the original physical imaging model based on the assumption that the attenuation coefficient of

the direct signal is mostly determined by the depth information. Consequently, compared with existing underwater image restoration methods, MonoUIR is based on a physically more accurate imaging model without losing feasibility. Its improvement can be mainly summarized into two aspects: (1) The direct signal and the backscattering signal depend on different attenuation coefficients. (2) The attenuation coefficient of the direct signal is adaptive to the depth. Ultimately, the model adopted by MonoUIR can be formulated as,

$$\boldsymbol{I}_c = \boldsymbol{D}_c + \boldsymbol{B}_c = \boldsymbol{J}_c * e^{-\boldsymbol{\beta}_c^D(\boldsymbol{z}) * \boldsymbol{z}} + \boldsymbol{A}_c * \left(1 - e^{-\boldsymbol{\beta}_c^B * \boldsymbol{z}}\right) \quad (2)$$

3.2. Depth Estimation

To eliminate the dependence on ranging equipment or multiple images, MonoUIR utilizes the monocular depth estimation and then scales the depth map with the maximum visible distance to obtain the absolute depth map. This strategy enables MonoUIR to perform restoration with only one RGB underwater image, and be applicable to more cases.

In MonoUIR, the outdoor monocular depth estimation algorithm [14] is adopted. Based on the pre-trained model on the KITTI dataset [15], we further fine-tune the model using two underwater RGBD datasets, seathru [11] and SQUID [10], to make the model more suitable for underwater scenarios. A typical sample of the estimated depth map of our scheme is illustrated in Fig. 2. From the figure, it can be seen that the depth map estimated by our monocular pipeline can achieve comparable accuracy with the ground truth.
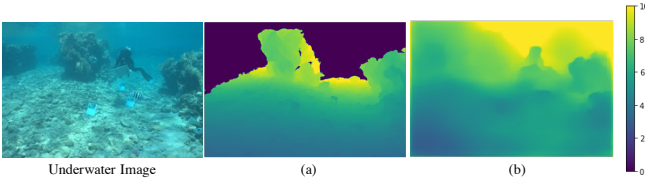
Fig. 2. The depth map (a) provided by RGBD dataset seathru [11] and (b) estimated by our monocular pipeline.

3.3. Backscattering Estimation

The estimation of the backscattering signal relies on the assumption [13] that the image intensity of black or completely shaded areas is entirely determined by the backscatter since there is no reflected light from the object itself. Based on this assumption, our backscattering estimation algorithm can be summarized as follows.

Firstly, ten equally spaced depth intervals are partitioned according to the upper and lower bounds of the depth map. Next, all pixels are grouped into ten sets $\boldsymbol{\omega}_1, \boldsymbol{\omega}_2, \ldots, \boldsymbol{\omega}_{10}$, in which the depth of the pixels in $\boldsymbol{\omega}_i$ is in the ith depth interval.

Then, the pixels whose average intensity of RGB channels is at the minimum of 1% on $\boldsymbol{\omega}_i$ are picked to form the set $\boldsymbol{\phi}_i$. And we define $\boldsymbol{\Phi} = \{\boldsymbol{\phi}_1, \boldsymbol{\phi}_2, \ldots \boldsymbol{\phi}_{10}\}$, where the pixels do

not have any reflected signal according to the above assumption, that is, $\boldsymbol{D}_c(\boldsymbol{\Phi}) \approx 0$. Based on this prior, pixels in set $\boldsymbol{\Phi}$ are used to fit the backscattering signal via non-linear least square optimization. The problem can be formulated as,

$$\min_{\boldsymbol{A}_c, \boldsymbol{\beta}_c^B} \left\| \widehat{\boldsymbol{B}_c}(\boldsymbol{\Phi}) - \boldsymbol{I}_c(\boldsymbol{\Phi}) \right\|_2 \quad (3)$$

where $\widehat{\boldsymbol{B}_c}$ is defined as,

$$\widehat{\boldsymbol{B}_c} = \boldsymbol{A}_c * \left(1 - e^{-\boldsymbol{\beta}_c^B * \boldsymbol{z}}\right) \quad (4)$$

In addition, we found that for the fitting in the green and the blue channel, the aforementioned non-linear model performs well, while for the red channel, the linear model is better, which is given as,

$$\widehat{\boldsymbol{B}_c} = \boldsymbol{A}_c * \left(1 - \boldsymbol{\beta}_c^B * \boldsymbol{z}\right) \quad (5)$$

3.4. Transmission Map Estimation

From Eq. (2), with the estimated $\boldsymbol{B}_c$, the restoration problem can be converted to the estimation of the transmission map $\boldsymbol{T}_c$, which is given as,

$$\boldsymbol{T}_c = e^{-\boldsymbol{\beta}_c^D * \boldsymbol{z}} \quad (6)$$

The direct signal $\boldsymbol{D}_c$ is actually the reflected signal $\boldsymbol{J}_c$ after the attenuation of $\boldsymbol{T}_c$. Inspired by retinex-based illumination estimation, the estimation of $\boldsymbol{T}_c$ can be simplified as the estimation of the illuminant map between the lens and the scene. In our implementation, the local space average color is calculated, and the steps can be summarized as follows.

To estimate the local space average color $\boldsymbol{l}_c(\boldsymbol{x})$ of the pixel $\boldsymbol{x}$ in channel c, the first step is finding its neighborhood set $\boldsymbol{N}_e(\boldsymbol{x})$, which can be described as,

$$\boldsymbol{N}_e(\boldsymbol{x}) = \{\boldsymbol{x}' \mid \|\boldsymbol{z}(\boldsymbol{x}) - \boldsymbol{z}(\boldsymbol{x}')\| \le \epsilon\} \quad (7)$$

where $\boldsymbol{z}(\boldsymbol{x})$ is the depth of $\boldsymbol{x}$, and ϵ is a constant threshold. Then, $\boldsymbol{l}_c(\boldsymbol{x})$ can be estimated iteratively by,

$$\boldsymbol{l}'_c(\boldsymbol{x}) = \frac{1}{|\boldsymbol{N}_e(\boldsymbol{x})|} \sum_{\boldsymbol{x}' \in \boldsymbol{N}_e(\boldsymbol{x})} \boldsymbol{l}_c(\boldsymbol{x}') \quad (8)$$

$$\boldsymbol{l}_c(\boldsymbol{x}) = \boldsymbol{D}_c(\boldsymbol{x}) * (1 - p) + \boldsymbol{l}'_c(\boldsymbol{x}) * p \quad (9)$$

where $\boldsymbol{l}_c(\boldsymbol{x})$ is initialized to zero, p controls how strong $\boldsymbol{l}_c(\boldsymbol{x})$ is affected by its neighbours. Next, $\boldsymbol{T}_c$ can be approximated as $\boldsymbol{l}_c$. Then, with the estimated $\boldsymbol{T}_c$, the rough estimation $\hat{\boldsymbol{\beta}}_c^D$ of the attenuation coefficient $\boldsymbol{\beta}_c^D$ can be given as,

$$\hat{\boldsymbol{\beta}}_c^D = -\frac{\ln \boldsymbol{T}_c}{\boldsymbol{z}} \quad (10)$$

To further refine the estimation of $\boldsymbol{\beta}_c^D$, the dependence between $\boldsymbol{\beta}_c^D$ and the depth map $\boldsymbol{z}$ is introduced in MonoUIR.

And the binomial exponential model is employed according to our data analysis. The problem is formulated as,

$$\boldsymbol{\beta}_c^D = a * e^{b*\boldsymbol{z}} + c * e^{d*\boldsymbol{z}} \quad (11)$$

$$\min_{a,b,c,d} ||\boldsymbol{\beta}_c^D - \hat{\boldsymbol{\beta}_c^D}||_2 \quad (12)$$

4. RUCB DATASET ESTABLISHMENT

Since it is challenging to simultaneously obtain a real underwater image and the corresponding ground truth of the same scene, researchers either obtain paired degraded images and references via synthetic techniques or collect them from manually built test tanks. By contrast, our full-reference dataset, RUCB, was collected completely in the real-world marine environment, allowing our RUCB to characterize underwater images more authentically compared to artificial datasets.

The standard color board, which contains 6 gray-scale patches and 18 colored ones, is utilized to be photographed both in the air and in various underwater environments. In this way, the color mapping relationship between the underwater images and the corresponding references can be established, which offers solid data support to the full-reference evaluation of the underwater image restoration schemes.

We collected underwater images from nine sites near the geographic coordinates (N29.483, E124.033) in the East China Sea. In order to collect underwater images at different depths, we fixed the color board and the water-proof camera on the same pole at distances of 0.5m, 1.0m, and 1.5m, respectively. Then we moved the pole down slowly until it was about 20 meters below the sea surface and captured underwater images with varying color tones produced by changing lighting. Images were all captured under natural light in the daytime between Jul. 31 and Aug. 3, 2021.

Finally, more than 20 videos were captured, covering a wide range of diversities on illuminations, depths of fields, blurring degrees, and color casts. We then cropped videos at intervals of 100 frames and filtered out the images whose color board is invisible. As a result, 2259 underwater images with noticeable differences were picked and paired with the corresponding reference images to establish RUCB dataset. To the best of our knowledge, this is the first full-reference underwater image dataset collected entirely in the real world.

5. EXPERIMENTAL RESULTS

5.1. Traits of Underwater Image Datasets

To more intuitively illustrate the advantages of our RUCB dataset compared with existing competitors, in Table 1, we summarize the characteristics of them from three aspects: the scale of the dataset, the acquisition way of underwater images and that of non-degraded references. From the table, it can be seen that RUCB is the largest one among all counterparts.

Table 1. Traits of underwater image datasets.

| Dataset	Scale	Underwater Images	References
UCCS [9]	300	real-world	/
UIEB [16]	890	real-world + sythetic	sythetic
SQUID [10]	41	real-world	/
seathru [11]	1157	real-world	/
TURBID [12]	300	test tank	test tank
RUCB (Ours)	2259	real-world	real-world

Moreover, it is also the only full-reference underwater image dataset collected entirely in the real-world environment.

5.2. Fitting Effectiveness

As aforementioned, for the backscattering estimation, the non-linear model performs satisfactorily in the green and blue channels, while for the red channel, the linear model will be better. Besides, as discussed in Sect. 3.4, the binomial exponential model is matched for the transmission map estimation. To qualitatively verify our claim, we provide the fitting results of three typical underwater images between the backscattering signal and the depth in Fig. 3. And Fig. 4 illustrates the relationship between the attenuation coefficient of the direct signal and the depth. From the results, our strategy is corroborated to be reasonable and effective.
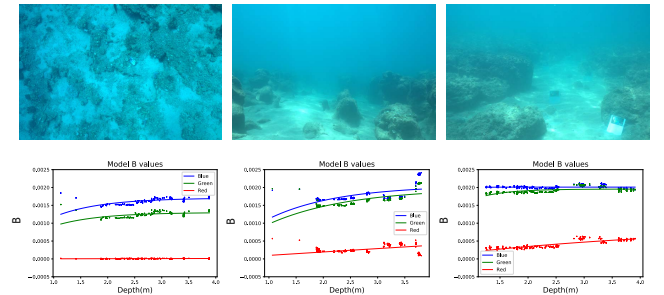
Fig. 3. The fitting results of the relationship between the backscattering signal and the depth in three typical samples.
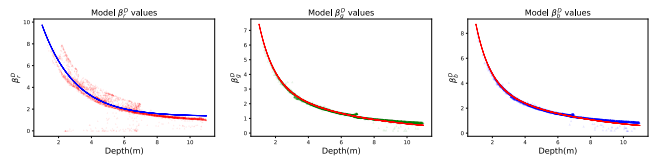
Fig. 4. Illustration of the relationship between the attenuation coefficient of the direct signal and the depth. From (a)~(c), the results for R, G, and B channels are given, respectively.

5.3. Comparison with the State-of-the-art Methods

In this subsection, we compare the performance of MonoUIR with five representative model-based restoration methods, in-

Table 2. Non-reference quantitative comparison results in terms of the average UCIQE and UIQM on the whole dataset.

Method	UCIQE↑			UIQM↑		
	UIEB	UCCS	SQUID	UIEB	UCCS	SQUID
DCP [17]	1.289	0.700	0.560	1.886	1.611	0.691
UDCP [3]	2.575	1.720	2.376	1.600	1.763	0.812
Li et al. [18]	1.617	1.095	0.770	**2.200**	2.461	1.009
IBLA [19]	1.426	0.445	/	1.381	1.467	/
ULAP [20]	1.437	0.767	0.570	1.939	2.199	0.973
MonoUIR(Ours)	**2.865**	**1.950**	**2.410**	1.961	**2.488**	**1.266**

cluding DCP [17], UDCP [3], Li *et al.* [18], IBLA [19], and ULAP [20]. For a fair comparison, the results of other methods were all generated by the official implementations.

Non-reference assessment on public datasets. In this part, three public underwater datasets, including UIEB [16], UCCS [9] and SQUID [10], were employed to evaluate the effectiveness of MonoUIR. Qualitative results are illustrated in Fig. 5. It can be observed that DCP [17], UDCP [3], IBLA [19] and ULAP [20] can only partially eliminate blur and color distortion, while Li *et al.* [18] overcompensates the attenuation of the red channel, resulting in an inharmonious red hue. By contrast, our MonoUIR produces finer textures and more natural colors, making the restored images closer to the real-world scene.
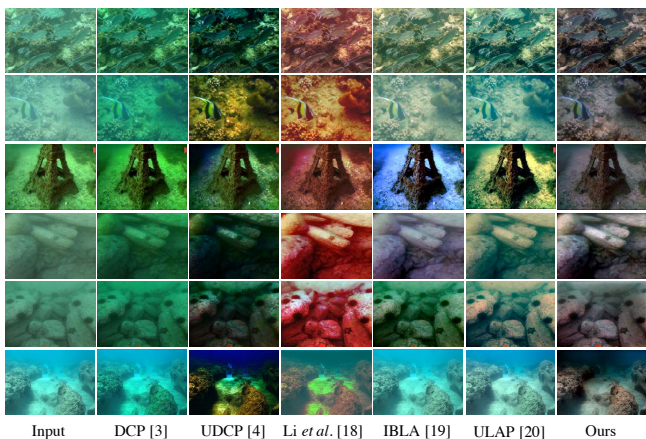

Fig. 5. Qualitative comparison results on public underwater datasets. The images in the first three rows are from the UIEB [16] dataset, followed by two rows from the UCCS [9] dataset and the last row from the SQUID [10] dataset.

To further quantitatively compare the performance of these restoration methods, two commonly used non-reference evaluation metrics, UCIQE [1] and UIQM [2], were calculated, and the results are summarized in Table 2. It can be seen that MonoUIR outperforms other compared methods by a large margin in terms of non-reference assessment.

Full-reference assessment on RUCB dataset. Based on our RUCB dataset, we further evaluated the color restoration performance of MonoUIR and other competing methods in a full-reference manner. The qualitative results are given in Fig.

6, where we can see that the colors restored by our MonoUIR are the closest to the reference at all tested depths. To quantitatively measure the deviation between the restored color and the ground truth, the CIEDE1976 chromatic aberration was employed as the metric. Table 3 reports the average chromatic aberration between the restored color and the reference captured in the air. It can be seen that MonoUIR has an overwhelming advantage compared with other counterparts at the depth of 0.5m and 1.0m. For images at the depth of 1.5m, although our MonoUIR is only slightly superior to Li *et al.*'s method [18], we found that this is mainly due to the overcompensation for red of Li *et al.*'s scheme [18], which makes it perform relatively well on the red-dominated color blocks. It can also be confirmed by Fig. 6. In summary, MonoUIR performs much better than other competitors in terms of full-reference assessment.
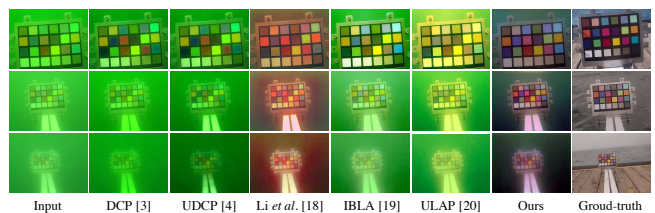
Fig. 6. Qualitative comparison on the RUCB dataset. The first image was photographed at the depth of 0.5m, followed by two images taken at the depth of 1.0m and 1.5m, respectively.

6. CONCLUSION

In this paper, we proposed a novel underwater image restoration solution, namely MonoUIR. Compared with existing methods, our MonoUIR employs a more physical-accurate and robust imaging model, in which the attenuation coefficients are signal-distinguished and adaptive to the depth of field. By integrating the monocular depth estimation, MonoUIR does not rely on any ranging equipment or specific shooting operations. Extensive experiments have demonstrated that MonoUIR achieves the best performance among all competitors both qualitatively and quantitatively. Furthermore, we established the first full-reference underwater dataset, RUCB, which was collected entirely in the real-world marine environment. It will offer solid data support to the full-reference assessment on the performance of underwater image restoration methods.

7. ACKNOWLEDGMENT

Table 3. Full-reference quantitative comparison results in terms of the average CIEDE1976(↓) on the whole RUCB dataset.

Color	Depth=0.5m						Depth=1.0m						Depth=1.5m					
(R, G, B)	DCP [17]	UDCP [3]	Li et al. [18]	IBLA [19]	ULAP [20]	Ours	DCP [17]	UDCP [3]	Li et al. [18]	IBLA [19]	ULAP [20]	Ours	DCP [17]	UDCP [3]	Li et al. [18]	IBLA [19]	ULAP [20]	Ours
(115, 82, 69)	71.390	53.246	60.881	85.457	69.235	**36.307**	73.774	71.984	49.969	87.781	73.714	**43.041**	90.711	80.224	42.842	108.175	81.113	**40.727**
(204,161,141)	72.775	57.866	71.740	84.755	70.538	**49.898**	82.406	89.105	56.530	75.454	65.401	**43.525**	86.636	88.185	**42.563**	86.710	69.684	52.890
(101,134,179)	75.569	61.885	70.326	90.093	67.692	**43.864**	86.834	88.915	58.537	87.204	76.760	**44.228**	94.382	88.197	45.025	102.456	76.322	**38.315**
(89,109,61)	66.466	54.399	67.981	86.568	69.741	**37.570**	72.993	76.661	53.260	86.075	78.331	**40.700**	84.491	76.582	42.672	104.424	80.126	**33.820**
(141,137,194)	75.177	58.342	68.498	93.154	64.095	**34.342**	91.713	94.308	58.473	89.196	80.118	**45.661**	95.221	91.005	44.319	100.835	78.631	**42.344**
(132,228,208)	73.148	64.084	65.749	88.790	64.047	**39.705**	89.474	102.620	69.275	78.234	78.712	**56.435**	82.564	86.727	**51.376**	81.221	70.037	54.506
(249,118,35)	60.025	46.907	59.325	71.090	59.626	**27.967**	79.748	81.142	**47.657**	81.720	59.856	55.617	89.200	84.790	**37.525**	97.845	74.955	57.084
(80,91,182)	62.998	42.895	50.546	74.899	60.329	**27.483**	84.731	77.966	54.699	91.939	76.995	**48.363**	99.973	84.607	46.005	113.894	82.103	**37.841**
(222,91,125)	62.911	46.147	66.708	74.417	59.888	**30.285**	84.785	80.707	51.075	86.797	60.336	**50.724**	96.828	87.461	**39.815**	103.964	78.581	46.527
(91,63,123)	62.967	41.761	49.450	75.887	55.597	**22.458**	75.617	67.448	49.974	90.720	73.153	**39.329**	95.792	79.525	47.081	115.242	83.910	**31.223**
(173,232,91)	63.802	57.765	73.024	85.480	74.193	**40.319**	76.687	65.321	66.329	65.208	67.575	**51.214**	67.597	75.139	**51.823**	73.407	65.699	55.762
(255,164,26)	62.850	49.590	61.442	75.728	58.786	**32.894**	78.547	86.094	53.883	77.739	64.181	**53.839**	81.812	82.064	**39.842**	89.534	74.931	52.303
(44,56,142)	59.675	36.787	35.340	62.377	46.764	**24.102**	76.687	65.321	46.891	90.792	72.634	**43.234**	97.240	78.245	46.801	116.855	83.367	**35.412**
(74,148,81)	60.320	49.713	67.032	88.209	64.953	**36.418**	69.024	78.392	59.932	76.923	72.927	**43.085**	76.554	74.142	45.036	93.412	70.347	**44.063**
(179,42,50)	54.798	39.165	45.537	70.930	50.455	**32.574**	77.274	68.240	48.816	91.796	63.019	**44.837**	95.845	79.459	44.326	113.175	85.805	**38.172**
(250,226,21)	68.174	61.247	70.994	77.060	73.712	**53.103**	68.348	83.306	60.145	63.187	57.871	**50.292**	68.737	77.608	**47.872**	69.235	62.375	61.128
(191,81,160)	61.560	43.572	58.756	77.325	53.658	**33.671**	87.394	83.318	52.748	89.834	69.773	**49.081**	100.626	89.570	44.489	109.525	83.746	**42.024**
(6,142,172)	64.605	53.541	49.248	72.045	65.653	**33.511**	81.219	85.202	62.092	86.562	82.476	**54.658**	87.047	80.670	**41.862**	100.131	76.132	45.768
(252,252,252)	83.170	77.598	65.744	85.574	69.154	**44.364**	94.252	107.451	65.469	68.597	72.738	**49.904**	88.877	92.807	**45.559**	79.871	67.981	51.344
(230,230,230)	76.520	69.455	62.359	78.372	61.521	**44.800**	91.273	103.399	63.210	69.189	69.506	**44.054**	90.931	93.482	46.115	81.344	69.211	**45.585**
(200,200,200)	71.448	63.636	62.198	75.354	60.178	**43.941**	89.508	100.436	62.739	71.154	67.759	**41.634**	89.501	92.853	46.045	79.878	67.522	45.592
(143,143,142)	65.451	53.443	68.391	83.225	66.662	**36.217**	83.283	91.916	59.867	75.655	65.226	**39.103**	89.225	89.496	46.134	86.499	71.173	**43.009**
(100,100,100)	60.121	41.755	49.004	73.911	55.780	**28.306**	78.618	84.392	56.733	80.159	71.556	**44.863**	86.618	82.585	40.827	94.855	73.212	40.629
(50,50,50)	54.727	31.287	28.117	60.897	36.583	**17.940**	70.571	68.486	**45.737**	86.540	73.410	47.797	88.384	75.268	38.287	110.533	82.244	**35.962**

8. REFERENCES

[1] M. Yang and A. Sowmya, "An underwater color image quality evaluation metric," *IEEE Trans. IP*, vol. 24, no. 12, pp. 6062–6071, 2015.

[2] K. Panetta, C. Gao, and S. Agaian, "Human-visual-system-inspired underwater image quality measures," *IEEE J. Ocean. Eng.*, vol. 41, no. 3, pp. 541–551, 2015.

[3] P. Drews, E. Nascimento, S. Botelho, and M. Campos, "Underwater depth estimation and image restoration based on single images," *IEEE Comput. Graph. and Appl.*, vol. 36, no. 2, pp. 24–35, 2016.

[4] H. Liu and L. Chau, "Underwater image restoration based on contrast enhancement," in *ICDSP*, 2016, pp. 584–588.

[5] Y. Peng, K. Cao, and P. Cosman, "Generalization of the dark channel prior for single image restoration," *IEEE Trans. IP*, vol. 27, no. 6, pp. 2856–2868, 2018.

[6] J. Li, K. Skinner, R. Eustice, and M. Johnson-Roberson, "Watergan: Unsupervised generative network to enable real-time color correction of monocular underwater images," *IEEE RA-L*, vol. 3, no. 1, pp. 387–394, 2017.

[7] C. Li, J. Guo, and C. Guo, "Emerging from water: Underwater image color correction based on weakly supervised color transfer," *IEEE Signal Process. Lett.*, vol. 25, no. 3, pp. 323–327, 2018.

[8] Y. Guo, H. Li, and P. Zhuang, "Underwater image enhancement using a multiscale dense generative adversarial network," *IEEE J. Ocean. Eng.*, vol. 45, no. 3, pp. 862–870, 2019.

[9] R. Liu, X. Fan, M. Zhu, M. Hou, and Z. Luo, "Real-world underwater enhancement: Challenges, benchmarks, and solutions under natural light," *IEEE Trans. CSVT*, vol. 30, no. 12, pp. 4861–4875, 2020.

[10] D. Berman, D. Levy, S. Avidan, and T. Treibitz, "Underwater single image color restoration using haze-lines and a new quantitative dataset," *IEEE Trans. PAMI*, vol. 43, no. 8, pp. 2822–2837, 2020.

[11] D. Akkaynak and T. Treibitz, "Sea-thru: A method for removing water from underwater images," in *CVPR*, 2019, pp. 1682–1691.

[12] A. Duarte, F. Codevilla, J. Gaya, and S. Botelho, "A dataset to evaluate underwater image restoration methods," in *IEEE Oceans*, 2016, pp. 1–6.

[13] D. Akkaynak and T. Treibitz, "A revised underwater image formation model," in *CVPR*, 2018, pp. 6723–6732.

[14] I. Alhashim and P. Wonka, "High quality monocular depth estimation via transfer learning," *arXiv preprint arXiv:1812.11941*, 2018.

[15] P. Geiger, A.and Lenz and R. Urtasun, "Are we ready for autonomous driving? the kitti vision benchmark suite," in *CVPR*, 2012, pp. 3354–3361.

[16] C. Li, C. Guo, W. Ren, R. Cong, J. Hou, S. Kwong, and D. Tao, "An underwater image enhancement benchmark dataset and beyond," *IEEE Trans. IP*, vol. 29, pp. 4376–4389, 2019.

[17] K. He, J. Sun, and X. Tang, "Single image haze removal using dark channel prior," *IEEE Trans. PAMI*, vol. 33, no. 12, pp. 2341–2353, 2010.

[18] C. Li, J. Quo, Y. Pang, S. Chen, and J. Wang, "Single underwater image restoration by blue-green channels dehazing and red channel correction," in *ICASSP*, 2016, pp. 1731–1735.

[19] Y. Peng and P. Cosman, "Underwater image restoration based on image blurriness and light absorption," *IEEE Trans. IP*, vol. 26, no. 4, pp. 1579–1594, 2017.

[20] W. Song, Y. Wang, D. Huang, and D. Tjondronegoro, "A rapid scene depth estimation model based on underwater light attenuation prior for underwater image restoration," in *Pacific Rim Conf. Multimedia*, 2018, pp. 678–688.